

Analysis of overload and sensorless control capability of PM-assisted synchronous reluctance machines

Original

Analysis of overload and sensorless control capability of PM-assisted synchronous reluctance machines / Leuzzi, R.; Cagnetta, P.; Ferrari, Simone; Pescetto, Paolo; Pellegrino, GIAN - MARIO LUIGI; Cupertino, F.. - ELETTRONICO. - (2017), pp. 172-178. (Intervento presentato al convegno Electrical Machines Design, Control and Diagnosis (WEMDCD), 2017 IEEE Workshop on tenutosi a Nottingham, United Kingdom, United Kingdom nel 20-21 April 2017) [10.1109/WEMDCD.2017.7947743].

Availability:

This version is available at: 11583/2675964 since: 2018-02-20T10:04:47Z

Publisher:

IEEE

Published

DOI:10.1109/WEMDCD.2017.7947743

Terms of use:

This article is made available under terms and conditions as specified in the corresponding bibliographic description in the repository

Publisher copyright

IEEE postprint/Author's Accepted Manuscript

©2017 IEEE. Personal use of this material is permitted. Permission from IEEE must be obtained for all other uses, in any current or future media, including reprinting/republishing this material for advertising or promotional purposes, creating new collecting works, for resale or lists, or reuse of any copyrighted component of this work in other works.

(Article begins on next page)

Analysis of Overload and Sensorless Control Capability of PM-Assisted Synchronous Reluctance Machines

R. Leuzzi, P. Cagnetta, S. Ferrari, P. Pescetto, G. Pellegrino, F. Cupertino

Abstract—Synchronous reluctance machines are a valid alternative to induction motors for industrial applications requiring variable speed regulation. To mitigate the well-known downside of their lower power factor, permanent-magnet-assisted topologies are adopted. Both high-strength rare-earth magnets and low cost ferrite magnets can be used in such machines. Their design and optimization procedures have been discussed in related literature. This paper compares synchronous reluctance machines assisted with NdFeB and ferrite magnets, focusing on torque overload capability and feasibility of saliency-based position estimation algorithms. Three prototypes were realized and tested. They all have the stator of a commercial induction motor, and three custom synchronous reluctance rotors with same laminations: one has no magnets, the other two have NdFeB and ferrite magnets respectively, designed to give the same torque at rated current. Results from simulations and experiments are presented, focusing on torque and demagnetization limits in the over-current loading range. Moreover, the feasibility of saliency-based sensorless methods is investigated, both at high and low current loads. The results of the paper suggest that the ferrite-assisted solution is the candidate solution for replacing induction motors in variable speed applications.

Index Terms—demagnetization, high-frequency voltage injection, overload, permanent magnet motor, sensorless control, synchronous reluctance motor.

INTRODUCTION

SYNCHRONOUS reluctance (SyR) machines are gaining increasing interest for variable-speed industry applications due to their low cost and high efficiency. Their efficiency is better than the one of an equivalent induction motor (IM) with same rating, because of the absence of rotor copper losses [1]. Moreover, the SyR motors exhibit good torque density and overload capability, leading their peak torque values to be comparable to those of permanent magnet synchronous machines. Magnetic saliency plays a critical role on the performance of such machines, also in term of flux-weakening capability, as described in [2].

Dealing with the design of SyR machines, torque ripple is one of main concerns. It is demonstrated in literature that if proper design measures are taken [3] and barrier shape optimization is performed [4], torque ripple can be drastically

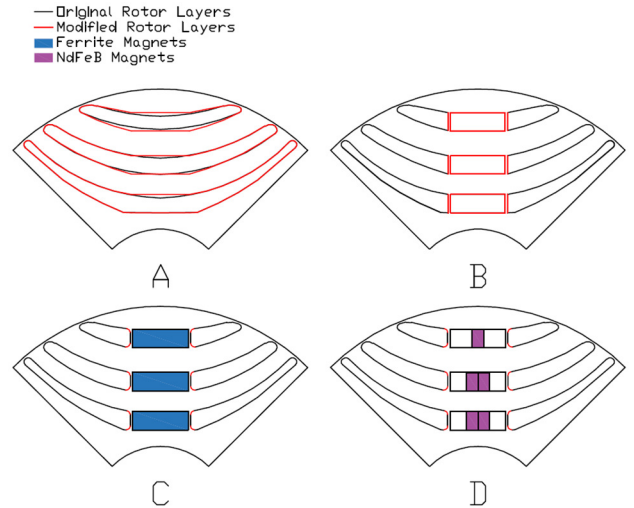


Fig. 1. Adaptation of barrier shape to insert the magnets: a) original, b) modified, c) with ferrite magnets, d) with NdFeB magnets.

mitigated. If needed by the application, skewing the rotor is also an effective measure to eliminate residual torque oscillations, as commonly done for IMs.

Another issue to be considered is the effect of the tiny iron ribs that structurally sustain the rotor flux carriers, because they shunt flux through the maximum reluctance direction and are ultimately the responsible for the low power factor of the SyR motor. To this purpose, the first substantial effect of permanent magnets (PMs) inserted within the flux barriers is to saturate the ribs and help improving the power factor. Moreover, the PMs produce additional flux linkage also yielding to an additional torque contribution [5]. The main torque contribution remains the one coming from the machine reluctance, and the described performance enhancement is obtained with a limited quantity of high-energy magnets, such as sintered NdFeB ones. Alternatively, similar results can be obtained inserting in the barriers a low strength magnet (e.g. ferrite), in greater quantity. Among permanent magnet materials, ferrites are very cheap, being very common iron oxides with a relatively simple extraction process. Ferrite magnets can tolerate temperatures up to 250 °C or 300 °C, a

This work was supported in part by the Italian Ministry of University and Research under Grant PON03PE_00067_8.

R. Leuzzi, P. Cagnetta, and F. Cupertino are with the Department of Electrical and Information Engineering, Politecnico di Bari, Bari, Italy (e-mail: riccardo.leuzzi@poliba.it).

S. Ferrari, P. Pescetto, and G. Pellegrino are with the Department of Energy, Politecnico di Torino, Torino, Italy (e-mail: gianmario.pellegrino@polito.it).

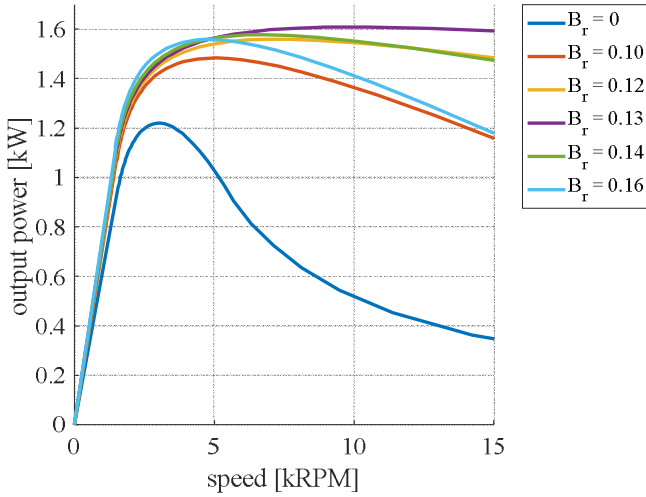


Fig. 2. Selection of magnet flux for the PM-assisted SyR motors.

feature that makes them suitable for application in harsh environments. Furthermore, their intrinsic coercivity increases as the temperature raises, making them more resistant to irreversible demagnetization. Conversely, neodymium magnets, generally have maximum operating temperatures of 120 or 150 °C, unless dysprosium is added with notable cost raise.

It is in this perspective that the designers and manufacturers have increasingly investigated solutions involving ferrite magnets in the last years, especially for those applications where the quantity of PM material is significant or for high volumes of production.

In this scenario, the aim of the present paper is twofold. The paper compares one SyR motor and of two PM-assisted SyR motors (ferrite and NdFeB magnets), at first in terms of their overload capability, including the analysis of robustness toward irreversible demagnetization and temperature effect. Second, the influence of the rotor type on saliency-based position detection is analyzed comparatively. It is commonly known that the high magnetic anisotropy of SyR motors is desirable also for zero-speed position detection approaches based on high-frequency (HF) signal injection. In these techniques, a HF voltage vector is superimposed to the control voltage applied by the inverter at the fundamental frequency. Referring to the HF model of the machine, the difference between the d- and q-axis incremental inductances affects the magnitude of the currents, which can in turn be measured to detect the rotor position [6].

A design procedure is presented, to select the proper amount of magnet to insert within the barriers to reach the same performance target at rated current. A detailed explanation of the HF sensorless techniques is made in [7] and [8], where also the influence of the rotor structure on saliency and cross-coupling is considered. An in-depth investigation of cross-coupling effects for transverse-laminated SyR machines can also be found in [9].

The results of the paper show that besides enhancing torque production and the power factor, the PM-assistance also makes the sensorless control more insensitive to the operating

point, avoiding dangerous operating points around zero torque. Moreover, the paper shows that the use of ferrite magnets is recommendable for industry applications, both for its lower cost and its higher overall performance.

II. DESIGN OF THE THREE MACHINES

This section deals with the design of the three prototypes under analysis. A commercial IM for general-purpose application is taken as a reference. Its rotor is replaced with custom designed rotors of the SyR type, while keeping the same stator, winding arrangement and self-ventilation cooling apparatus. The performance target for all three designs is 1.1 kW rated power at 1500 rev/min, i.e. a rated torque of 7 Nm.

A. Design of the SyR Rotor

The first design step is the optimization of the rotor barriers geometry. Of all possible degrees of freedom describing the barriers geometry the attention was focused on those parameters that mostly influence the anisotropy ratio (i.e. average torque production) and the torque ripple. Different rotor barrier shapes and numbers of barriers per pole were considered, eventually leading to a rotor with three barriers per pole coupled with the original 36-slots, 4-poles IM stator.

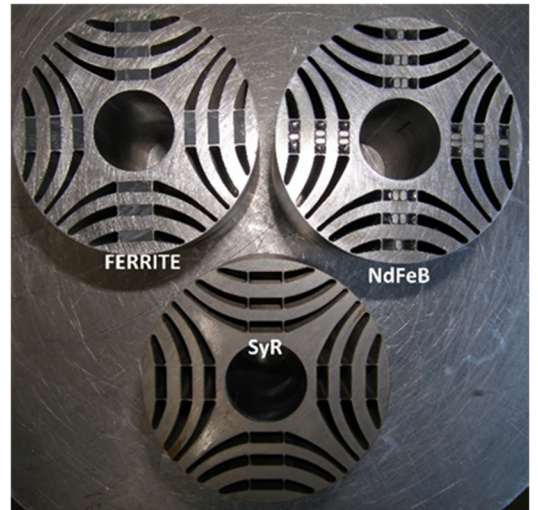


Fig. 3. Picture of the three rotors assembled.

The barriers shape is inspired to the field lines in a solid rotor, using the conformal mapping theory, as suggested in [5]. The design was aided by multi-objective optimization algorithm pursuing the best compromise between average torque and torque ripple. Finite element analysis (FEA) was used during the optimization. More details on the design steps can be found in [4]. The optimized SyR rotor is reported in Fig. 1a and referred to as the one with “original rotor layers”.

B. Permanent Magnet Design

The second step in the PMa-SyR rotors design process deals with the permanent magnets quantity and geometry. For the sake of simplicity, the barriers are initially supposed completely filled with a fictitious permanent magnet material

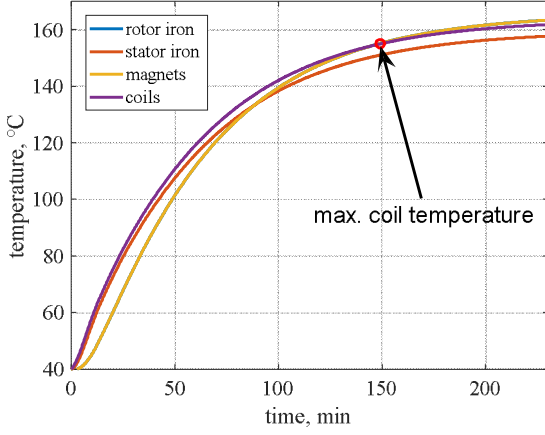


Fig. 4. Simulated thermal transient of the various parts of the ferrite-assisted SyR motor, at 40 °C ambient temperature when a current twice the rated one is supplied.

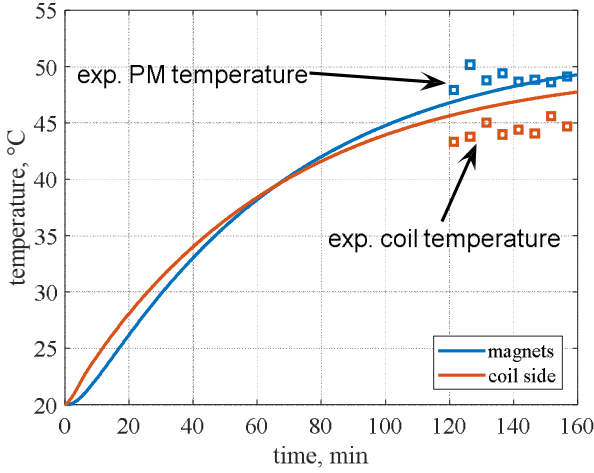


Fig. 5. Experimental validation of the thermal model: motor driven at 1500 rev/min at rated current.

having remanence B_r' and parallel magnetization direction. The design parameter B_r' can be used to calibrate the power versus speed characteristic of the machine, at rated current and limited inverter voltage are reported. Fig. 2 reports the power profile for different values of B_r' . In the considered example, the widest constant power speed range is obtained with $B_r' = 0.13$ [T]. A further increase of magnet strength (e.g. $B_r' = 0.16$ [T]) would lead to a small power increase at low speed, associated to a power drop at maximum speed. Therefore, the condition $B_r' = 0.13$ [T] will be used in the following for determining the final shape and volume of the NdFeB and ferrite magnets.

C. Final Magnets

Unless cast bonded magnets are considered, the solution of Fig. 1a, with the barriers totally filled with PM material is hardly manufacturable. A valid alternative is to replace the $B_r' = 0.13$ [T] bonded magnet with smaller pieces of higher strength magnetic material, namely rectangular pieces of commercial ferrite or NdFeB.

Say the volume of one barrier is V_r' and the remanence of

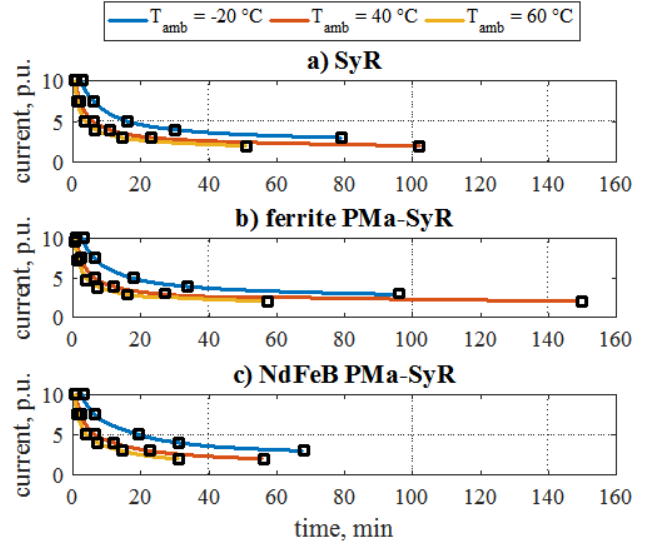


Fig. 6. Maximum overload time with respect to overload current for the three motors under study (simulation data).

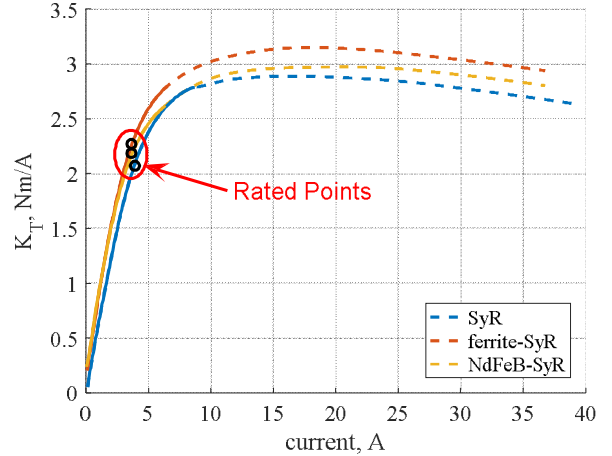


Fig. 7. Torque constant K_t as a function of current (peak values) for the three machines under study: continuous line are experimental data, dashed lines are simulation results.

the final magnet is B_r , the volume of the new magnet V_r can be found by the simple proportion

$$V_m = V_m' \cdot \frac{B_r'}{B_r} \quad (1)$$

Two PMa-SyR rotors have been realized following this principle, one with ferrite BMHF-32/32 magnets ($B_r = 0.41$ T) and one with BMN-38H(S) NdFeB magnets ($B_r = 1.22$ T). The original rotor layers were modified so to accommodate the rectangular ferrite magnets, as told by the reference “modified rotor layers” in Fig 1a. Finally, radial ribs were added (Fig. 1b) to avoid magnet displacement and to improve the mechanical robustness. Radial ribs thickness was kept equal to the minimum tolerance allowed by the laser cut technology adopted to realize the prototypes. Three rotor stacks were manufactured according to the final design reported in Fig. 1b. One was left with no magnets. The second and the third one have ferrite (Fig. 1c) and NdFeB (Fig. 1d)

magnet pieces, respectively. Fig. 3 shows a picture of the stacks of the three rotors. Although in principle the magnet pieces of the three layers would need individual optimization both PM-assisted solutions use magnets having all the same shape. This was decided for cost and simplicity reasons. The ferrite magnets have a cross section area of $12 \times 4 \text{ mm}^2$, whereas the dimensions of the NdFeB magnets $2.5 \times 4 \text{ mm}^2$.

III. TORQUE OVERLOAD CAPABILITY

The limiting factors for the overload capability of a machine are the maximum temperatures that the different parts can tolerate and, in the case of PM motors, the risk of magnets demagnetization. Commercial motors for general-purpose application are commonly manufactured with class F winding insulation, having a maximum admissible temperature of 155°C . Since the SyR motor has no magnets, and the selected ferrite PMs can tolerate up to 250°C , the temperature limit of the windings was considered as the maximum admissible temperature for the analysis. Conversely, the selected neodymium magnets present a maximum operating temperature of 120°C , therefore this value has been used as rotor temperature limit in case of the neodymium-assisted motor.

A. Transient Overload Analysis

This first study aims at evaluating the transient overload capability of the three machines, considering the temperature limit and the demagnetization limit. To the purpose of the study, the parameters related to the cooling system have been modeled in the FEA software MotorSolve, namely the fan dimensions and the air flow rate. The analysis is carried out at three different ambient temperatures, namely -20 , $+40$ and $+60^\circ\text{C}$. Several simulations have been performed at different loads for all three ambient temperatures, referring to the maximum torque per ampere (MTPA) control law and rated speed. The transient temperature response of the main components of the machine was analyzed, using a lumped parameter thermal network. As an example, Fig. 4 shows the temperature response of the ferrite-SyR machine, when starting from a room temperature of 40°C , applying twice as much the rated current value. The temperatures of the different parts follow each other closely, with the windings and magnets having the highest values. The time when windings or magnets reach their temperature limit defines the overload time for the considered current overload condition. In the example of Fig. 4, the coils reach a temperature of 155°C after 150 minutes. To validate the thermal model employed, the ferrite-SyR motor has been driven at rated load and speed for 160 minutes. Results are shown in Fig. 5 and compared with the simulation results from the thermal model at the same conditions. Fig. 6 summarizes the overload time as a function of the load levels, with the ambient temperature as parameter.

The SyR and ferrite PMa-SyR motors can withstand overload conditions for longer than the NdFeB PMa-SyR motor, due to the more stringent temperature limit dictated by the neodymium magnets. On average, ferrite PMa-SyR motors withstand overload conditions almost 20% longer than the NdFeB PMa-SyR motor with 60°C ambient temperature. Finally, Fig. 6 tells that the one per-unit current condition does not necessarily coincide with continuous operation limit. This

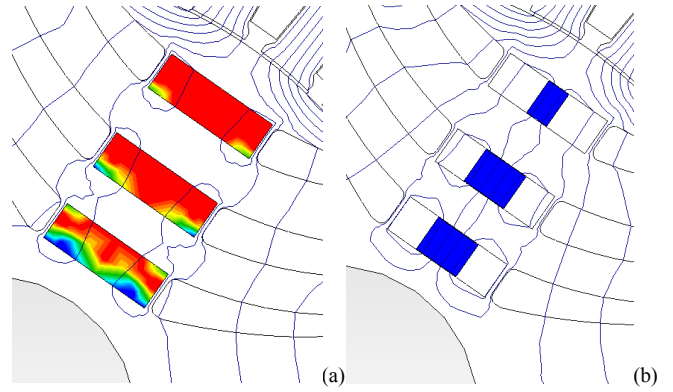


Fig. 8. Demagnetization prediction for (a) ferrite magnets and (b) neodymium magnets at 40°C ambient temperature, 9.2 A (peak) supplied in q-axis direction.

TABLE I. MAX OPERATING CURRENT CONSIDERING DEMAGNETIZATION

Ambient temperature	-20°C	40°C	60°C
Ferrite magnet	11.3 A	9.2 A	8.5 A
NdFeB magnet	$>40 \text{ A}$	$>40 \text{ A}$	$>40 \text{ A}$

is common for high efficiency class motors (IE3 and above). The choice of the ambient temperature levels comes from the operative range required by the standard IEC 60034-30-1, which regulates the requirements for low-voltage motors employed in industrial applications. Standards also refer to 40°C as the rated ambient temperature during normal operating conditions, therefore it is common use to refer nominal data to this value.

B. Nm per ampere analysis

Expectedly, the PM-assisted machines absorb lower current values than the SyR machine, to develop the same rated torque. Fig. 7 shows the torque constant K_T [Nm/A] as a function of the phase current amplitude. This result was experimentally verified up to 8 A, controlling the motors in MTPA conditions. Values of the torque constant at higher current levels were calculated with FEA simulations and reported with dashed lines in Fig. 7.

It is interesting to notice that both PM-assisted motors were designed so to give the same torque at rated current (namely 8 Nm at 3.6 A, peak value, i.e. 2.22 Nm/A). They do actually perform very similarly up to the rated current value, but the characteristic of the NdFeB PMa-SyR tend to saturate earlier in overload conditions, due to temperature rise and local saturation phenomena that occur in the rotor iron near the barriers, as confirmed from FEA.

C. Demagnetization Limit

The demagnetization state has been checked for each operating point, and no risk has been found when the motors are operated along their MTPA characteristic, for all the considered values of overload current. To further investigate the demagnetization limits of the two PM-assisted machines, dedicated FEA simulations were performed, with the stator current opposed to the direction of the PMs. Results are reported in Table I, where the maximum current prior to demagnetization (peak value) is indicated for the two PMa-SyR motors, considering three different room temperatures. The thermal network was used again to determine the steady-

state temperature of the magnets. Neodymium magnets are very robust towards demagnetization in the considered current range while ferrite magnet cannot exceed two and a half times the rated current with 60 °C room temperature.

Fig. 8a and 8b show the contour plot of the demagnetization prediction for the ferrite and the neodymium PMa-SyR, respectively, considering a room temperature of 40 °C and a current of about three and a half times the rated one. The magnet can be considered irreversibly demagnetized in the red parts of its volume, while it is still healthy in the blue areas. These results visually confirm the higher robustness of NdFeB magnets toward demagnetization.

IV. SENSORLESS CONTROL CAPABILITY

The abundant saliency of the SyR machines can be profitably used for the sensorless estimation of the rotor position at low and zero speed operation. Very often, high-frequency (HF) voltage injection is used to inspect the machine saliency and determine the rotor position and speed. Different approaches have been proposed, but in most of them the response of the machine to the HF excitation signal is demodulated and used in a position tracking loop. As an example, Fig. 9 reports the block diagram of one possible position observer, based on pulsating HF voltage injected into the machine estimated d-axis \hat{d} (maximum permeance axis) and demodulation of the HF component of a current manipulation on the orthogonal axis.

SyR and PMa-SyR machines offer a good level of magnetic anisotropy, if compared to the other types of synchronous machines. Therefore, they are inherently suitable for zero-speed sensorless control based on signal injection. However, rotor saliency may vary with the operating point in the (d, q) current plane, due to saturation, leading to sensitivity to the operating point and possible loss of information in certain operating conditions. Such phenomenon was studied in [10] for internal PM motors. Besides that, the SyR motor presents specific issues in the low current region, which are solved by PM-assisted machines. To clarify this, the equations describing the machine response to alternating HF voltage signals are reported so to evidence the impact of machine's parameters on sensorless control capability. The injected voltage in the estimated reference frame is:

$$\begin{cases} v_{\hat{d}HF} = u_c \cdot \cos(\omega_c t) \\ v_{\hat{q}HF} = 0 \end{cases} \quad (1)$$

The \hat{q} component of the current vector contains information about the rotor position error $\tilde{\theta} = \theta - \hat{\theta}$ signal, and can be used to feed the tracking loop:

$$i_{\hat{q}HF} = \frac{u_c \sin(\omega_c t)}{2\omega_c (l_d l_q - l_{dq}^2)} \left[(l_d - l_q) \sin(2\tilde{\theta}) - 2l_{dq} \cos(2\tilde{\theta}) \right] \quad (2)$$

where l_d , l_q and l_{dq} are the incremental inductances of the machine. If the position error is small ($\tilde{\theta} \approx 0$) and neglecting the second term of the difference in the square brackets, the demodulated signal obtained from (2) can be approximated as:

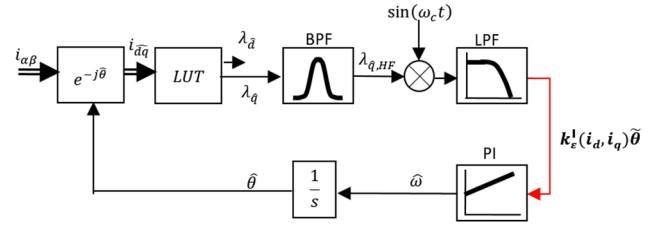


Fig. 9 Sensorless estimation of the rotor position using pulsating HF voltage injection. The key parameter $k_\epsilon(i_d, i_q)$ is in evidence.

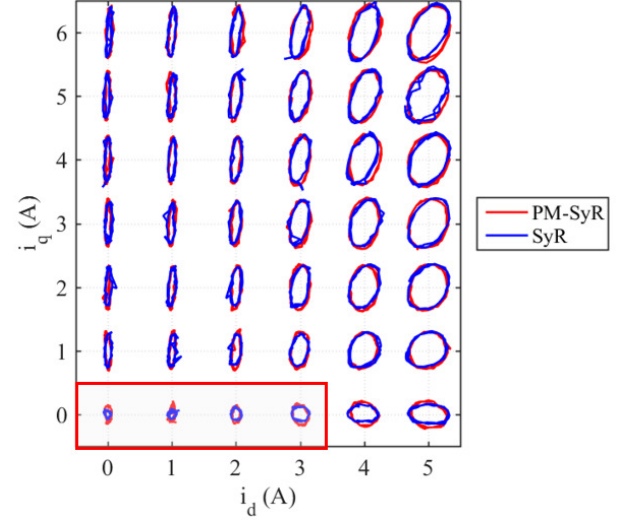


Fig. 10 Saliency analysis of SyR and NdFeB PMa-SyR motors, experimental results.

$$i_{\hat{q}HF, dem} \cong \frac{1}{2} k_\epsilon(i_d, i_q) \sin(2\tilde{\theta}) \cong k_\epsilon(i_d, i_q) \cdot \tilde{\theta} \quad (3)$$

The parameter k_ϵ is a function of the incremental inductances of the machine, and ultimately, of the state of excitation of the machine defined by i_d, i_q :

$$k_\epsilon(i_d, i_q) = \frac{u_c (l_d - l_q)}{2\omega_c (l_d l_q - l_{dq}^2)} \quad (4)$$

This technique is widely used in literature for PM motors, characterized by low cross-saturation effect [11]. For highly salient machines the term $2l_{dq} \cos(2\tilde{\theta})$ neglected in (2) will produce a position estimation error due to cross-saturation. This error can be overcome if the \hat{q} component of the estimated flux is demodulated in place of the current component, as in [12]. In this case, the error amplitude factor k'_ϵ (see Fig. 9) becomes, without approximations:

$$k'_\epsilon(i_d, i_q) = \frac{u_c}{2\omega_c} \frac{l_q (l_d - l_q) - 2l_{dq}^2}{l_d l_q - l_{dq}^2} \quad (5)$$

In the case of rotating voltage signal injection in stationary $\alpha\beta$ reference frame, it can be expressed in complex notation as:

$$v_{\alpha\beta HF} = u_c \cdot e^{j\omega_c t} \quad (6)$$

Current response to this signal is an ellipse made of a

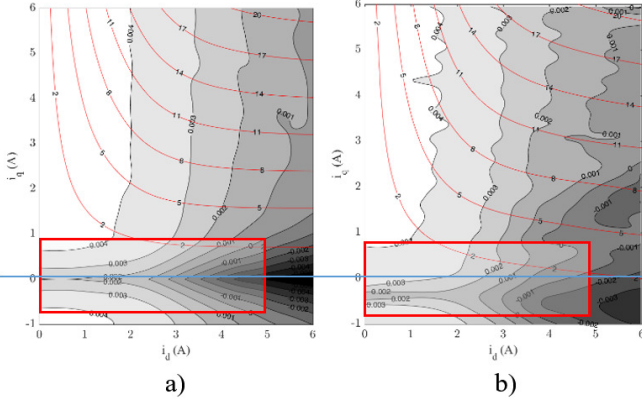


Fig. 11 k'_e contours: a) SyR; b) NdFeB-assisted SyR.

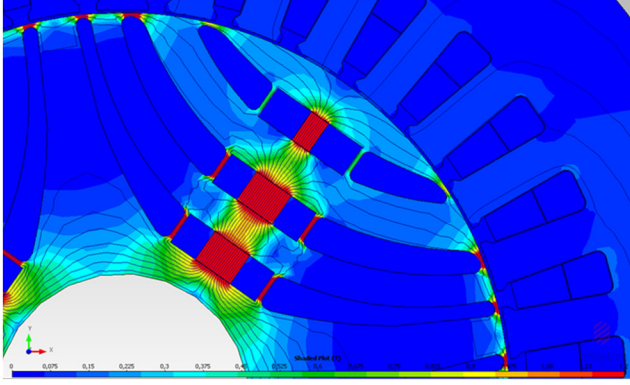


Fig. 12 FEM model of NdFeB-assisted SyR motor at zero current.

rotating positive sequence component I_{pos} , plus a counter rotating, negative sequence component I_{neg}

$$i_{\alpha\beta HF} = I_{pos} \cdot e^{j(\omega_c t - \frac{\pi}{2})} + I_{neg} \cdot e^{-j(\omega_c t - 2\theta - \varepsilon_{dq} + \frac{\pi}{2})} \quad (7)$$

where $\varepsilon_{dq} = \tan^{-1}(2l_{dq}/(l_d + l_q))$. The argument of the negative sequence current component contains the rotor position θ plus the angular deviation due to cross saturation ε_{dq} . The amplitude I_{neg} is a function of the operating point:

$$I_{neg}(i_d, i_q) = \frac{u_c \sqrt{(l_d - l_q)^2 + 4l_{dq}^2}}{2\omega_c (l_d l_q - l_{dq}^2)} \quad (8)$$

A. Saliency analysis and inspection

A dedicated experimental test was performed to investigate the machine saliency characteristic in the whole (d, q) current plane. Each motor under test was kept at stand-still, and fundamental i_d, i_q were imposed to define the operating point under investigation. A HF rotating voltage was superimposed to the fundamental voltage signals at the output of current PI regulators. Under these conditions, the current vector follows an elliptic trajectory because of the saliency, as reported in Fig. 10. For each working point, the ellipse eccentricity gives visual representation of the machine saliency: the more pronounced and vertical is the ellipse main axis, the more feasible and accurate will be sensorless control. Where the ellipse eccentricity is smaller, the saliency is lower. Where the

orientation of the ellipse is not vertical, there is a deviation produced by the cross-saturation effect. If manufacturing asymmetries are not considered, results can be considered to be independent of rotor position since a (d, q) reference frame is employed. Results in Fig. 10 refer to the SyR and to the NdFeB PMa-SyR motors, for comparison purpose. The two machines present almost the same saliency characteristic in most of the (d, q) current plane, except for the area highlighted in the red rectangle, where the SyR machine tends to become not salient whereas PMa-SyR machine maintains a reasonable level of saliency. Similar conclusions can be found when the gain k'_e is analyzed in the i_d, i_q plane. In Fig. 11, the k'_e parameter has been computed using (5) and based on the experimentally measured flux-current characteristics. SyR and neodymium PMa-SyR motors are compared. A high value of k'_e corresponds to high signal-to-noise ratio for sensorless control, while a negative k'_e leads to instability. As it can be seen, for the SyR machine the area in the red rectangle of Fig. 11, correspondent to low i_q , is critical since k'_e drops. The addition of the magnets in PMa-SyR machine shifts the critical region to negative i_q values, allowing stable sensorless operation even in no-load conditions.

B. Effect of bridge saturation

The effects described above can be explained considering the rotor structure of the two machines. If i_q is low and there are no magnets, the structural ribs are not saturated and therefore the flux crosses the rotor as if there were no flux barriers. In other words, under those circumstances the reluctance in the q -axis is unexpectedly low and the same is true for the machine saliency. This phenomenon harms the stability of sensorless control of SyR at low speed in no-load conditions. The problem is overcome by imposing a minimum excitation current or flux to the machine. If sufficient current is given in the d -axis, the ribs tend to saturate thanks to the cross-saturation effect, thus leading the machine saliency to acceptable levels.

In the PM assisted machines, the magnets have the precious function of saturating the ribs, also at zero current. This can be seen in Fig. 12, and also in the k'_e map of Fig. 11b, where the critical area around zero q current is shifted downwards, out of the operating quadrant. With PM-assistance, low-speed sensorless position estimation can be performed even at no-load without any need of a minimum flux excitation.

V. SUMMARY AND CONCLUSIONS

This paper focused on performance analysis of SyR and PM-assisted SyR motors in overload conditions and on their sensorless control capability at zero speed. Three prototypes were realized to replace the rotor of a commercial IM, and tested. The adoption of PM-assisted solutions not only improves the efficiency and power factor, but also enhances the magnetic saliency at low current levels, with advantages for sensorless position detection. It was demonstrated that SyR motor assisted by ferrite magnets guarantees the best overload performances in terms of torque production capability thanks to the higher operating temperature of the ferrite magnets. On

the other hand, the SyR motors assisted by neodymium magnets is more robust towards demagnetization. Both considered PM-assisted solutions appear as viable alternatives to IMs to improve not only its efficiency but also its overload performances and sensorless control capability with limited impact on cost.

REFERENCES

- [1] A. Boglietti, A. Cavagnino, M. Pastorelli and A. Vagati, "Experimental comparison of induction and synchronous reluctance motors performance," Fourtieth IAS Annual Meeting. Conference Record of the 2005 Industry Applications Conference, 2005., 2005, pp. 474-479 Vol. 1.
- [2] W. L. Soong and T. J. E. Miller, "Field-weakening performance of brushless synchronous AC motor drives," in *IEEE Proceedings - Electric Power Applications*, vol. 141, no. 6, pp. 331-340, Nov 1994.
- [3] A. Vagati, M. Pastorelli, G. Francheschini and S. C. Petrache, "Design of low-torque-ripple synchronous reluctance motors," in *IEEE Transactions on Industry Applications*, vol. 34, no. 4, pp. 758-765, Jul/Aug 1998.
- [4] G. Pellegrino, F. Cupertino and C. Gerada, "Automatic Design of Synchronous Reluctance Motors Focusing on Barrier Shape Optimization," in *IEEE Transactions on Industry Applications*, vol. 51, no. 2, pp. 1465-1474, March-April 2015.
- [5] N. Bianchi, E. Fornasiero and W. Soong, "Selection of PM Flux Linkage for Maximum Low-Speed Torque Rating in a PM-Assisted Synchronous Reluctance Machine," in *IEEE Transactions on Industry Applications*, vol. 51, no. 5, pp. 3600-3608, Sept.-Oct. 2015.
- [6] G. Scarcella, G. Scelba and A. Testa, "High performance sensorless controls based on HF excitation: A viable solution for future AC motor drives?," 2015 IEEE Workshop on Electrical Machines Design, Control and Diagnosis (WEMDCD), Torino, 2015, pp. 178-187.
- [7] M. Harke, H. Kim and R. D. Lorenz, "Sensorless control of interior permanent magnet machine drives for zero-phase-lag position estimation," *IEEE Transaction on Industry Applications*, vol. 39, no. 12, pp. 1661-1667, Nov./Dec. 2003.
- [8] N. Bianchi, S. Bolognani, J. H. Jang and S. K. Sul, "Comparison of PM Motor Structures and Sensorless Control Techniques for Zero-Speed Rotor Position Detection," in *IEEE Transactions on Power Electronics*, vol. 22, no. 6, pp. 2466-2475, Nov. 2007.
- [9] A. Vagati, M. Pastorelli, F. Scapino and G. Franceschini, "Impact of cross saturation in synchronous reluctance motors of the transverse-laminated type," in *IEEE Transactions on Industry Applications*, vol. 36, no. 4, pp. 1039-1046, Jul/Aug 2000.
- [10] N. Bianchi and S. Bolognani, "Influence of Rotor Geometry of an IPM Motor on Sensorless Control Feasibility," in *IEEE Transactions on Industry Applications*, vol. 43, no. 1, pp. 87-96, Jan.-feb. 2007.
- [11] J. Holtz, "Acquisition of Position Error and Magnet Polarity for Sensorless Control of PM Synchronous Machines," *IEEE Transactions on Industry Applications*, Vol. 44, n. 4, July-Aug. 2008 Page(s):1172 – 1180.
- [12] A. Yousefi-Talouki; P. Pescetto; G. Pellegrino, "Sensorless Direct Flux Vector Control of Synchronous Reluctance Motors Including Standstill, MTPA and Flux Weakening," in *IEEE Transactions on Industry Applications*, vol. PP, no. 99, pp.1-1.

BIOGRAPHIES

Riccardo Leuzzi (S'17) received the M.Sc. in electrical engineering in 2016 from the Politecnico di Bari, Bari, Italy, where he is currently working toward the Ph.D. degree in the field of converters, electric machines and drives.

Paolo Cagnetta received the B.Sc. and the M.Sc. in electrical engineering in 2011 and 2013, respectively, from the Politecnico di Bari, Bari, Italy. Since 2013, he has been with the Politecnico di Bari as research assistant in the field of electric machine design and testing. He is currently with the Distretto Tecnologico Aerospaziale in collaboration with AvioAero.

Simone Ferrari received the M. Sc. in electrical engineering from Politecnico di Torino, Turin, Italy in 2016, where he is currently working towards his PhD in electrical engineering. His PhD research project deals with the development of multi-physical and open-source design tools for electrical machines, especially for synchronous reluctance and PM-assisted synchronous reluctance machines.

Paolo Pescetto is a PhD student at the Politecnico di Torino, Turin, Italy. He received the B.Sc. and M.Sc. degrees from the same university in 2013 and 2015, respectively, with full grade and honours in both cases. In 2015, he was an Erasmus+ student at the Norwegian University of Science and Technology, Trondheim, Norway. His research interests include synchronous motor drives, sensorless control, and self-commissioning techniques. Mr. Pescetto has three conference papers. He received the Best Paper Award in Renewable Energies at the EVER15 conference and the Best Paper Award at the ICEM2016 conference.

Gianmario Pellegrino (M'06–SM'13) received the M.Sc. and Ph.D. degrees in electrical engineering from the Politecnico di Torino, Turin, Italy, in 1998 and 2002, respectively. He was a Guest Researcher with Aalborg University, Aalborg, Denmark, in 2002. Since 2002, he has been with the Politecnico di Torino, first as a Research Associate and then as an Assistant Professor since 2007. He was a Visiting Fellow with Nottingham University, Nottingham, U.K., in 2010/2011. He has published more than 50 technical papers and one patent. His research areas include electrical machines and drives. Dr. Pellegrino is an Associate Editor of the IEEE TRANSACTIONS ON INDUSTRY APPLICATIONS. He was a corecipient of the IEEE Industry Applications Society (IAS) Electric Machines Committee Third Best Paper Award at the IEEE Energy Conversion Congress and Exposition (ECCE) 2009, the IEEE IAS Industrial Drives Committee Third Best Paper Award at ECCE 2010, and the IEEE International Conference on Electrical Machines 2010 Best Paper Award.

Francesco Cupertino (M'08–SM'12) received the Ph.D. degree in electrical engineering from Politecnico di Bari, Bari, Italy, in 2001. Since then, he has been with the Department of Electrical and Information Engineering, Politecnico di Bari, where he is currently a Full Professor. His research interests include the design of synchronous electrical machines, intelligent motion control of electrical machines, applications of computational intelligence to control, and sensorless control of ac electric drives. He is the author or co-author of more than 100 scientific papers on these topics. Dr. Cupertino co-received the Prize Paper Award from the IEEE Industry Applications Society Electrical Machines Committee in 2014 and from the IEEE Industrial Electronics Society Electrical Machines Committee in 2015.